CrossMark

Microstructural and Mechanical Properties of Friction Stir Welded Nickel-Aluminum Bronze (NAB) Alloy

T. Küçükömeroğlu, E. Şentürk, L. Kara, G. İpekoğlu, and G. Çam

In this study, the applicability of friction stir welding to cast NAB alloy (i.e., C95800) with a thickness of 9 mm has been investigated. The joint performance was determined by conducting optical microscopy, microhardness measurements, and mechanical testing (e.g., tensile and Charpy impact tests). The effect of stir intensity on joint performance was also determined. A grain refinement (equiaxed fine grain structure) as well as evolution of a Widmanstätten structure was achieved within the stir zone of all the joints produced. Thus, all of the joints produced exhibited higher proof stress (i.e., between 512 and 616 MPa) than that of the base material, i.e., 397 MPa. On the other hand, only half of the specimens exhibited higher tensile strength values than that of the base plate (i.e., 794 MPa), whereas the other specimens displayed lower tensile strength than the base plate due to the existence of weld defects, namely cold bonding and/or tunnel defect.

1. Introduction

Cast NiAl bronze (NAB) alloys possess useful combinations of mechanical properties such as strength, toughness, and corrosion resistance (Ref 1, 2). Therefore, they are important naval alloys which are used extensively in propulsion and sea water handling systems. As-cast NAB alloys usually exhibit a microstructure consisting of coarse Widmanstätten α-phase containing Ni-Fe-Al κ-phases and island martensite β′ phase. They also contain some porosity as the case in other cast materials, which in turn have reduced properties and service performance. Moreover, the physical metallurgy of NAB alloys is complex and a wide range of transformation products form during cooling depending on the details of the thermal history (Ref 1). The bcc β-phase transforms to the fcc primary α-phase with a Widmanstätten morphology beginning at ∼1030 °C. At 930 °C, nucleation of globular κ_{ii}, which is nominally Fe_3Al with a DO_3 structure, starts in the β-phase. When the temperature reaches 860 °C, fine κ_{iv} precipitates, which are also nominally Fe_3Al, begin to form in the α-phase. The remaining β decomposes by the eutectoid reaction β → α + κ_{iii} at ∼800 °C, resulting in the formation of a lamellar constituent. The κ_{iii} is nominally NiAl with a B2 structure. Proeutectoid κ_{iii} may exhibit a globular morphology, or may form by epitaxy on the globular κ_{ii}. When the cooling rates are increased to ∼1 K s^{-1} or greater, the rapid cooling suppresses the eutectoid reaction. And therefore the Widmanstätten

morphology of the α-phase as well as bainitic and martensitic products of β-phase decomposition may become apparent (Ref 1). Thus, the fusion welding of these materials poses several difficulties, such as high distortion, cracking, and/or loss of toughness in heat-affected zone (HAZ) due to the formation of transformation products of β-phase as a result of fast cooling.

Several investigations have recently been conducted on friction stir processing (FSP), a solid-state processing technique, of these materials (Ref 3-10). For instance, Oh-Ishi et al. (Ref 3-7) reported that the microstructures of the friction stir processed NAB (Cu-9Al-5Ni-4Fe-1Mn; UNS C95800) was inhomogeneous, including Widmanstätten structure, equiaxed fine grain structure, and banded or lamellar structure, implying incomplete dynamic recrystallization as it is the case in other dual-phase Cu alloys (Ref 10-12). Although the predominant refinement effect is the dynamic recrystallization due to severe deformation resulting from the FSP in these multiple phase alloys as well, the material self characteristics should be considered for explaining the inhomogeneous structure of the onion ring observed in the NZ. For the banded structure, substructure and annealing twins were apparently visible within the α grains, indicating that the recovery and recrystallization occurred simultaneously with phase transformations during FSP. Furthermore, Oh-Ishi et al. (Ref 6) reported that many low-angle boundaries were observed in the upper region of the NZ, implying that part of the α-phase was retained without dynamic recrystallization during FSP. They also reported that the processing parameters affected the microstructure and temperature distribution in the friction stir processed NAB apparently. Mahoney et al. (Ref 8) and Fuller et al. (Ref 9) also studied the microstructure of friction stir processed NAB, and they reported similar microstructures to those reported by Oh-Ishi et al. (Ref 3-7). Similarly, a more recent study conducted by Ni et al. (Ref 10) has also demonstrated that the microstructure of the friction stir processed as-cast NAB was greatly refined and inhomogeneous in the NZ, indicating incomplete dynamic recrystallization. Moreover, significantly higher transverse tensile properties than the base plate can easily be achieved for FSP cast NAB alloys due to the fact that FSP effectively closes up the porosities and refines the

T. Küçükömeroğlu, E. Şentürk, and **L. Kara**, Department of Mechanical Engineering, Karadeniz Technical University, Trabzon, Turkey; and **G. İpekoğlu** and **G. Çam**, Department of Mechanical Engineering, Iskenderun Technical University, Iskenderun, Hatay, Turkey. Contact e-mail: gurelcam@gmail.com.

Table 1 Chemical composition of the NAB alloy used

Elements	Cu	Al	Ni	Fe	Mn	Sn	Si	Zn	Others
%	78.31	10.92	4.86	3.99	1.31	0.23	0.16	0.13	0.09

Others Zr, Co, Pb, Mg, Be, and Cr

microstructure in these cast alloys as it is the case in the cast Mg alloys (Ref 2, 13, 14).

It can be seen from the discussion above that the studies conducted on the as-cast NAB alloys are limited only to FSP and there is no report on FSW of these alloys in the open literature. However, friction stir welding (FSW) which is a solid-state joining technique offers a possibility for joining these materials without the problems encountered in fusion welding (Ref 2, 13-16). Furthermore, friction stir welding may lead to the elimination of the existing porosities in these as-cast materials in addition to the grain refinement in the weld region, which may in turn improve the mechanical properties. Furthermore, the range of the FSP parameters (rotation rate and traversing speed) studied to date is relatively narrow. Moreover, although there is no report in the literature on FSW of these alloys, it is expected that FSW will produce joints with mechanical properties higher than or comparable to those of the base plate in these cast alloys. Thus, there is certainly a need for further research to fully understand the effect of FSW parameters on microstructure and mechanical properties of the cast NAB alloys. This was the motivation for the conduction of the current study.

2. Experimental Procedure

Cast 78%Cu-11%Al-5%Ni-4%Fe NAB alloy (i.e., C95800) with a thickness of 9 mm was the base material used in this study, the chemical composition of which is given in Table 1. Since there is no literature on FSW of NAB alloys, the weld parameters were determined from the FSP studies reported in the literature. A stirring tool, with a conical pin having a triangular cross section without threads, made of WC was used, Fig 1. The pin outer diameters at the root and at the tip were 8 and 6 mm, respectively. The length of the pin was 8.5 mm and the diameter of the shoulder was 16 mm. The reason for choosing this stirring tool in the current study is the fact that this featureless conical pin reduces traversing forces and forging forces. In addition, it produces friction stir welds with satisfactory tensile test results (Ref 17). On the other hand, this pin being featureless does not have tread wear problem like featured pins. Various rotational rate and weld speed combinations were used in order to investigate the effect of stir intensity (i.e., the ratio of rotation rate to weld speed) on the joint microstructures and properties, Table 2. For this purpose, three groups of welded joints were planned, the first group being the joints produced at the rotational rate of 800 r min^{-1} using two different weld speeds, namely 85 and 135 mm min^{-1}. The second group of joints was produced using traverse speeds of 135 and 270 mm min^{-1} at the rotational rate of 1250 r min^{-1}. The last group of joints was obtained using the welding speeds of 135 and 270 mm min^{-1} at the rotational rate of 1600 r min^{-1}. All of the joining trials
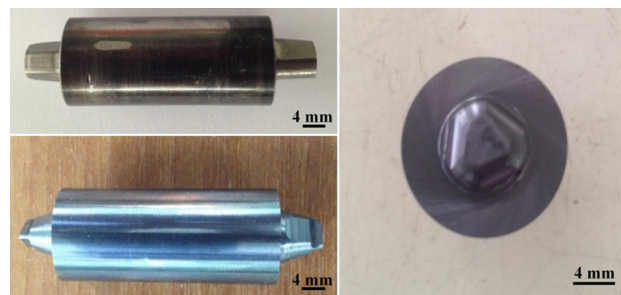

Fig. 1 Side and top views of the stirring tool used in this study

were made using a vertical milling machine under the load control mode using an axial force of 4500 N. Axial force was measured and controlled by a load cell system consisting of four load cells mounted on the table of the milling machine.

Metallography specimens were extracted from the welded plates for microstructural observations. Metallography specimens were polished with alumina solution in two steps (grain sizes being 1 and 0, 3 μm) and then etched also in two steps using solutions of 40 mL ammonium hydroxide (NH$_4$OH) and 20 mL hydrogen peroxide (H$_2$O$_2$) in 40 mL distilled water and 30 mL phosphoric acid (H$_3$PO$_4$) and 10 mL hydrogen peroxide (H$_2$O$_2$) in 60 mL distilled water, for one and two seconds, respectively. A detailed microstructural observation was conducted for each welded plate using optical microscopy and scanning electron microscopy (SEM) to determine the presence of any weld defect and the microstructural evolution within the stirred zone. Furthermore, microhardness measurements were conducted on each welded plate to determine hardness variations across the weld area of the joints obtained, using a load of 100 g for 10 seconds.

Moreover, transverse tensile test specimens, the geometry of which is shown in Fig. 2 (according to Turkish Standards, i.e., TS-138), were extracted from both base plates and all welded plates (minimum 3 specimens) and tested at room temperature (loading rate being 1 mm min^{-1}) to determine the joint performances. Moreover, three standard Charpy specimens (8 × 8 × 55 mm) were also extracted from each welded plate in order to determine the toughness values of the weld regions of the joints.

3. Results and Discussion

3.1 Microstructure

The microstructure of the as-cast base material used in this study is shown in Fig. 3. It consists of Cu-rich α-phase (a mixture of Widmanstätten alpha and globular alpha phases) and Ni-Fe-Al (κ) phase. Four types of κ-phase may be encountered in NAB alloys depending on the chemical composition of the

alloy. However, κ_I phase has only been observed in the alloys having an iron content exceeding 5%. The alloy used in this study has an iron content less than 5%, therefore κ_{II} phase is present within the alpha grains and they have a globular appearance as seen in Fig. 3.

The cross sections of the joints produced are shown in Fig. 4. The increasing stir intensity reduces or completely eliminates weld defects at all the rotational rate levels used in this study, namely 800, 1250, and 1600 r min^{-1}, and thus improves the joint quality. For example, specimen 800/135/4500 contains a higher amount of tunnel-like defects in addition to the cold bonding area. On the other hand, specimen 800/85/4500 contained a reduced amount of tunnel-like defect and no cold bolding area. Besides, the tunnel-like defect observed in the specimen 1600/270/4500 completely disappeared in the

specimen 1600/135/4500. The presence of these weld defects can be attributed to the fact that the weld speed is too high for the corresponding rotational rate. Thus, the stir intensity used is not sufficient for obtaining a sound joint.

A grain refinement in stir zone was observed in all the joints produced with different stir intensities, i.e., high and low, due to the extreme plastic deformation taking place, Fig. 5. Similar results were also reported for friction stir processed cast NAB alloys (Ref 3-10). Moreover, the occurrence of grain refinement within the stir zone was also reported for pure Cu and other Cu alloys as well (Ref 11, 12, 18-22). In addition to grain refinement in the stir zone, large globular κ_{II} particles observed in alpha matrix in the base material were broken up into smaller particles and distributed within both dynamically crystallized zone (DXZ) and thermo-mechanically affected zone (TMAZ) regions of the joints due to the excessive plastic deformation taking place during FSW. The grain size of the recrystallized grains within the stir zone was observed to increase with increasing stir intensity. This is possibly due to the increased heat input values in higher stir intensities since a higher stir intensity at constant rotation rate means that the weld speed is lower. Therefore, when the weld speed is lower, i.e., higher stir intensity condition, the tool has more time to heat the unit length of the workpiece than when the weld speed is higher, i.e., lower stir intensity condition. Moreover, it is also worth to point out that a Widmanstätten structure evolves in the DXZ of joints produced with higher stir intensities (Fig. 5a), while this structure decreases or completely disappears in the DXZ of the joints obtained with lower stir intensities (Fig. 5b). The presence of a Widmanstätten structure in the DXZ of friction stir processed NAB alloys was also reported in the literature (Ref 3-7).

SEM investigations also indicated that κ-phases, i.e., κ_{II}, κ_{III}, and κ_{IV}, were also present in the stir zone of the joints produced. Energy-dispersive spectroscopy (EDS) analyses results of these κ-phases, i.e., κ_{II}, κ_{III}, and κ_{IV}, and a SEM micrograph showing the particles on which EDS analyses conducted are shown in Fig. 6.

3.2 Hardness

Figure 7 illustrates the hardness profiles obtained from all the joints produced. As seen from this figure, a hardness increase in the stir zone was observed in all the joints, and the hardness value of the base material, i.e., about 290 HV, has

Table 2 Weld parameters used

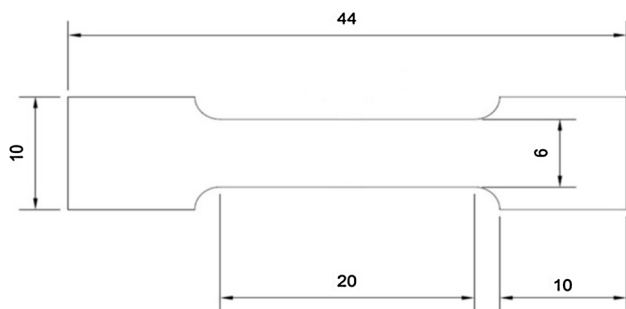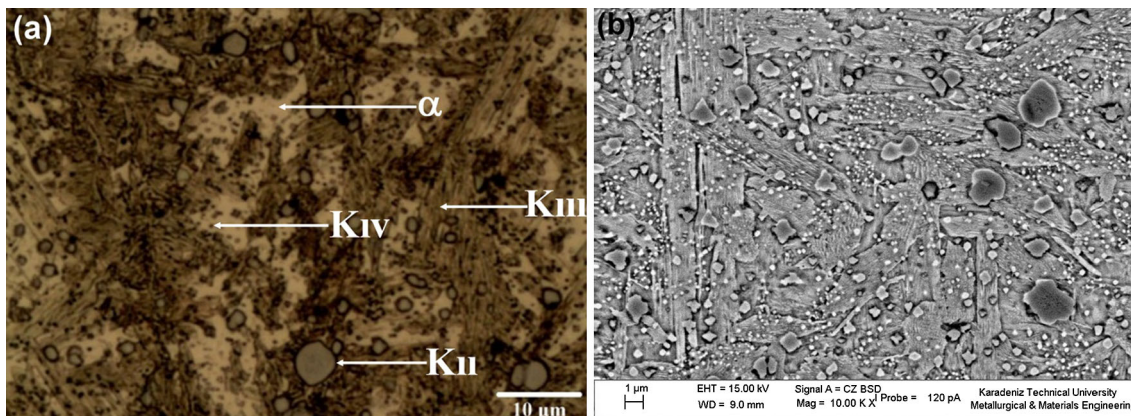| Specimen	Rotation rate (r min^{-1})	Weld speed (mm.min^{-1})	Axial force (N)	Stir intensity (r mm^{-1})
800/85/4500	800	85	4500	9.4
800/135/4500		135	4500	5.9
1250/135/4500	1250	135	4500	9.2
1250/270/4500		270	4500	4.6
1600/135/4500	1600	135	4500	11.8
1600/270/4500		270	4500	5.9

Fig. 2 Schematic illustration of the tensile test specimens used in this study (all dimensions are in mm and the thickness is 2 mm)

Fig. 3 Microstructure of the as-cast base material used in this study: (a) optical microscope image and (b) SEM image
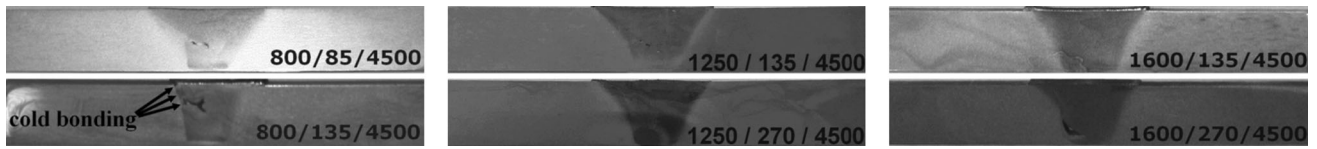
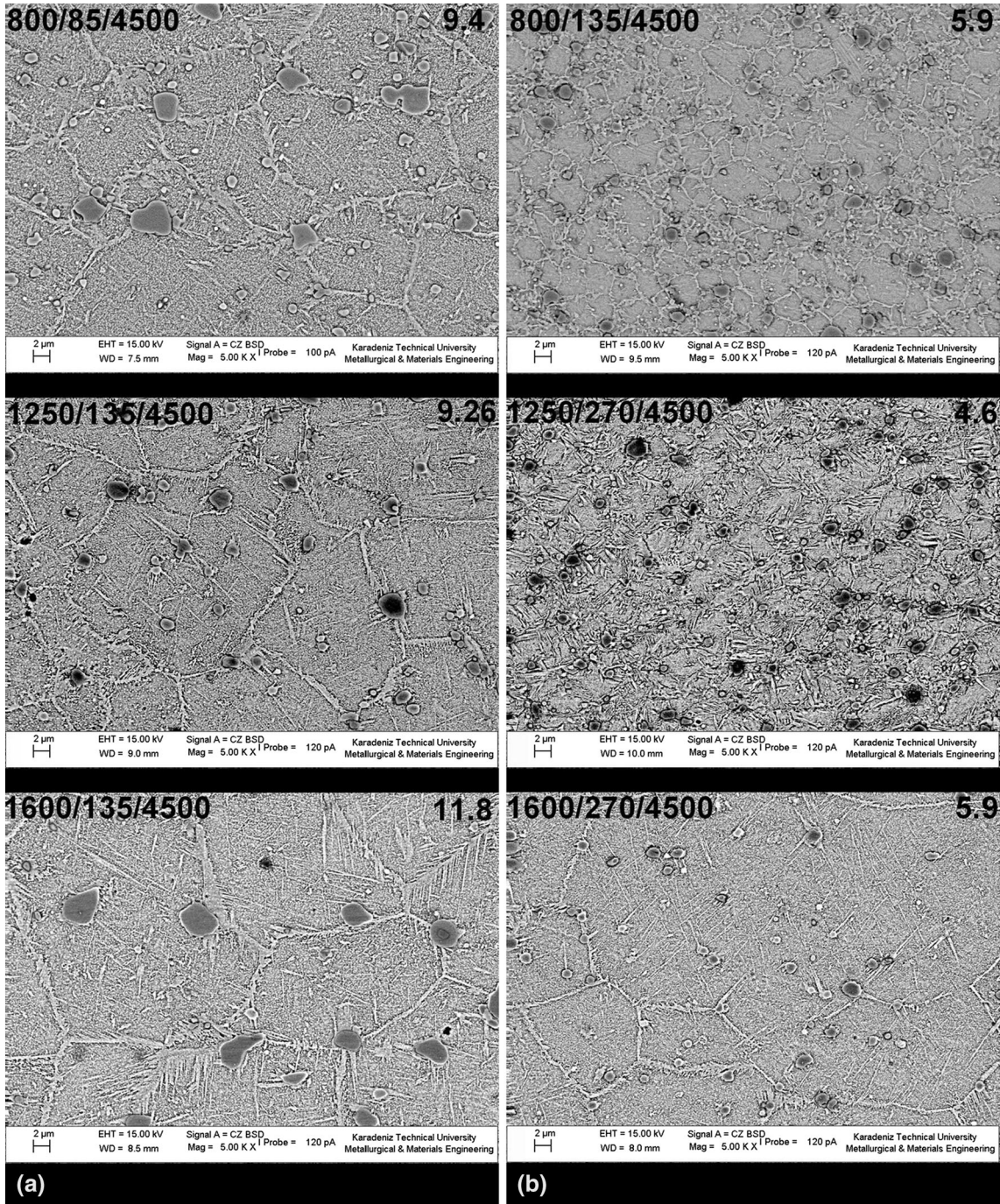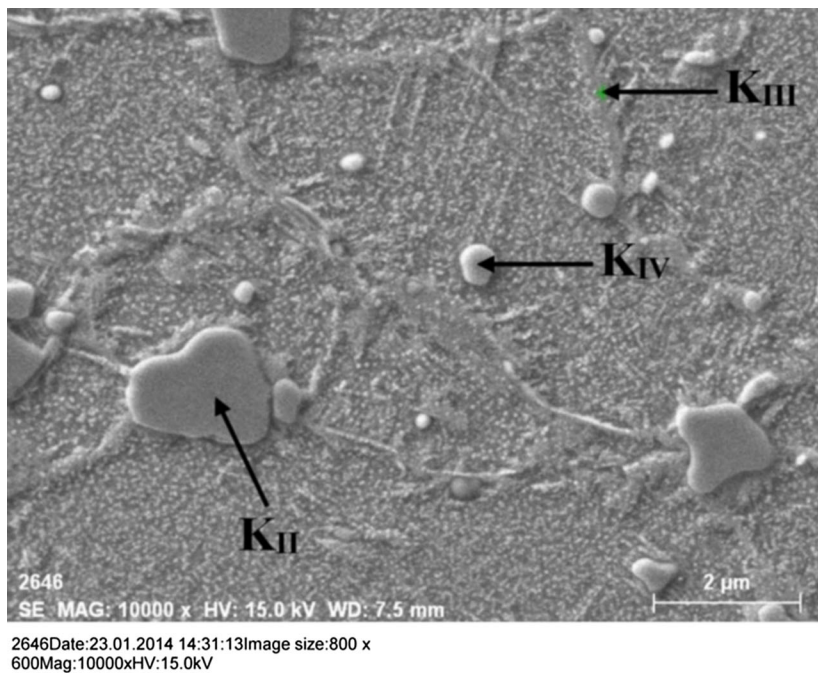**Fig. 4** Cross section of the joints obtained

Fig. 5 Microstructures of the stir zones of the joints produced with different stir intensities: (a) high stir intensity and (b) low stir intensity

been increased up to 395 HV. Similarly, a hardness increase was also reported for FSP cast NAB alloys by several researchers (Ref 3-10). Moreover, similar hardness increases

in the weld zone of FSW Al alloys in O-temper condition were also reported in the literature (Ref 23-28). The increase of hardness in the stir zone of the joints can partly be attributed to

Fig. 6 SEM analysis of the κ-phases in the stir zone
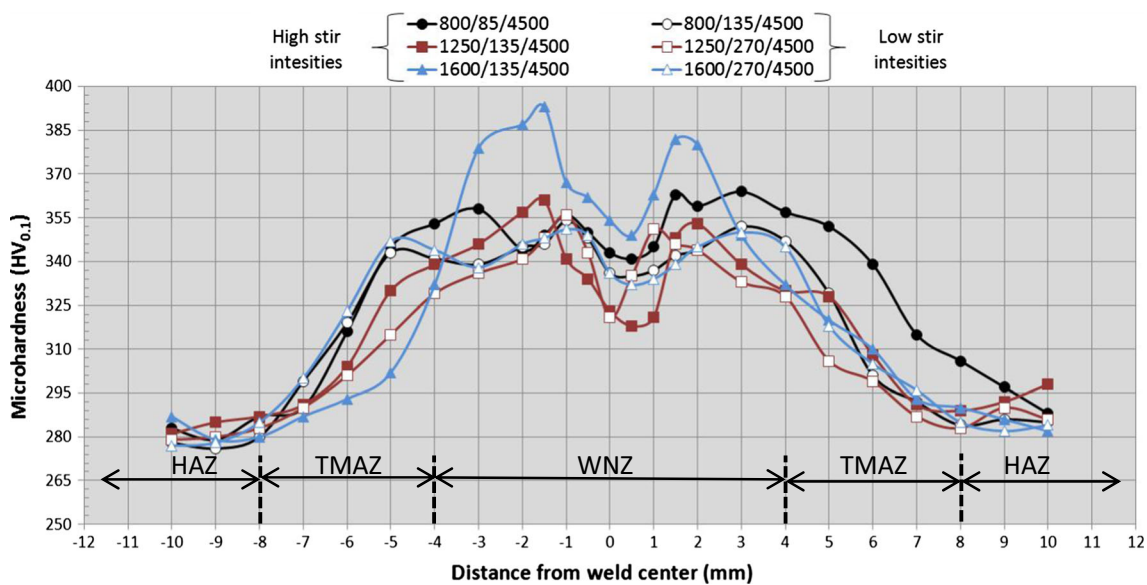
Fig. 7 Hardness profiles of the joints produced with different stir intensities

Table 3 Summary of the mechanical test results conducted both on base material and the joints obtained

Specimen	Stir intensity (r mm^{-1})	0.2% proof stress (MPa)	Tensile strength (MPa)
As-cast base material	...	397	794
800/85/4500	9.4	616	888
800/135/4500	5.9	545	549
1250/135/4500	9.2	588	732
1250/270/4500	4.6	512	757
1600/135/4500	11.8	555	868
1600/270/4500	5.9	552	850

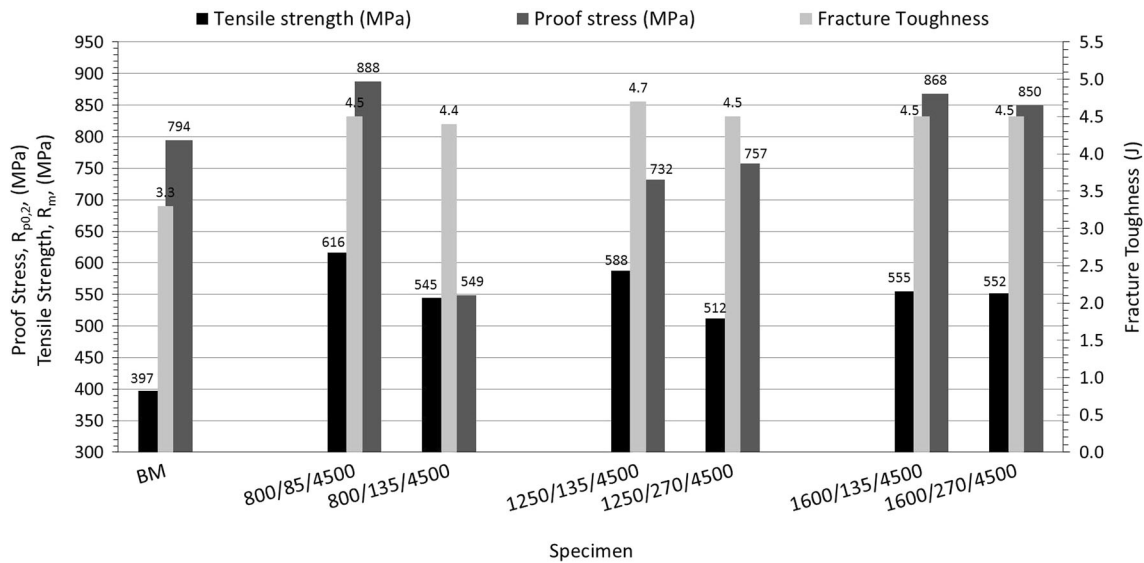**Fig. 8** Column graphic illustrating the tensile properties and Charpy test results of base material and all the joints produced with different stir intensities

the grain refinement taking place within this region after FSW as well as homogeneous distribution of fine κ_{II} particles throughout the microstructure. However, the degree of hardness increase in the weld region depends on the stir intensity. The degree of hardness increases as the stir intensity increases. It is worth pointing out that although the specimens produced using higher stir intensities exhibit a coarse grain structure than the specimens obtained with lower stir intensities, they display higher hardness values. This contradiction can be explained by the microstructure evolving in the weld zones of the specimens produced with different stir intensities. As mentioned earlier, a Widmanstätten structure evolves in the DXZ of joints produced with higher stir intensities (Fig. 5a) thus leading to higher hardness values. Moreover, the hardness decreases slightly in the middle of weld region (near the central line) for all the joints. The reason for this hardness decrease is probably the excessive break-up of large globular κ_{II} particles into smaller particles in this region due to the excessive plastic deformation taking place during FSW. But the hardness in this region is still much higher than that of the as-cast base plate.

3.3 Mechanical Properties

Table 3 provides a summary of the tensile tests results conducted both on base material and the joints obtained. Figure 8 also gives a column graphic showing tensile test results. As seen from Table 3 and Fig. 8, all the joints produced exhibited higher proof stress values than that of the base alloy due to hardness increase in the weld zone. Among all the joints, the 800/135/4500 specimen displayed the lowest tensile strength values. As mentioned earlier in the microstructure section (Fig. 4), this joint exhibited highest amount of weld defects, i.e., cold bonding in addition to the tunnel defect, in the weld area. Therefore, fracture took place within the weld region where defects are present in this specimen, thus exhibiting lower tensile strength than all other joints produced in this study. All other joints fractured within the HAZ. The reason for this is that the reduced section of transverse tensile specimens extracted from the joints (20 mm long) contained only weld nugget, TMAZ, and a small portion of the HAZ region on each

side. Thus, the fracture took place where the strength was the lowest in the reduced section of transverse tensile specimens, namely HAZ region, Fig. 7. Moreover, although some of these joints contained weld defects in the DXZs, they fractured also in the HAZ region exhibiting tensile strength values similar or higher than that of the base alloy. This can be attributed to the fact that a hardness increase takes place in the DXZs of these joints, thus giving a shielding effect. It is, however, worth pointing out that the mechanical properties reported here were obtained by testing the reduced sections of transverse tensile specimens as mentioned earlier. Thus, the mechanical properties of the joints may somewhat differ provided that standard transverse tensile specimens extracted from the joints are tested.

Charpy test results are also shown in Fig. 8. As seen from this figure, all the joints produced in this study exhibited similar fracture toughness values, i.e., between 4.4 and 4.7 Joules, although some of them contained some weld defects. Thus, this suggests that the presence of some weld defects does not play an important role in determining the fracture toughness since a fine-grained microstructure evolves in the weld area of these joints. Moreover, all the joints displayed higher fracture values than the base alloy, i.e., 3.3 Joules. This can also be attributed to the formation of a fine-grained structure within the weld regions of the joints, suggesting that this fine-grained structure evolved in the weld region exhibits better toughness as well as strength than the as-cast base plate.

4. Conclusions

As-cast NAB alloy (i.e., C95800) with a thickness of 9 mm was successfully butt-joined using friction stir welding using various weld parameter combinations, i.e., stir intensities. A grain refinement within the stir zone was observed in all the joints produced due to the excessive plastic deformation and simultaneous recrystallization taking place during FSW. The joints produced using higher stir intensities exhibited a Widmanstätten structure, and this structure decreased or

completely disappeared as the stir intensity decreased. All the joints obtained exhibited a hardness increase within the weld region. This hardness increase can be attributed to the evolution of a Widmanstätten structure as well as to grain refinement taking place within the weld region. The fracture took place outside DXZ in most of the joints although they contain some weld defects in the DXZ, due to the shielding effect provided by the hardness increase. All the joints produced exhibited similar or higher tensile strength and fracture toughness values than the as-cast base alloy.

References

1. ASM handbook, Welding, Brazing and Soldering, vol. 6, ed. by D.L. Olsonet al (ASM International, Materials Park, 1993)
2. G. Çam, Friction Stir Welded Structural Materials: Beyond Al-alloys, *Int. Mater. Rev.*, 2011, **56**(1), p 1–48
3. K. Oh-Ishi, A.M. Cuevas, D.L. Swisher, and T.R. McNelley, The Influence of Friction Stir Processing on Microstructure and Properties of a Cast Nickel-Aluminum Bronze Material, *Mater. Sci. Forum*, 2003, **426–432**, p 2885–2890
4. K. Oh-Ishi and T.R. McNelley, Microstructural Modification of As-Cast NiAl Bronze by Friction Stir Processing, *Metall. Mater. Trans. A*, 2004, **35A**, p 2951–2961
5. K. Oh-Ishi and T.R. McNelley, The Influence of Friction Stir Processing Parameters on Microstructure of As-Cast NiAl Bronze, *Metall. Mater. Trans. A*, 2005, **36A**, p 1575–1585
6. K. Oh-Ishi, A.P. Zhilyaev, and T.R. McNelley, A Microtexture Investigation of Recrystallization During Friction Stir Processing of As-Cast NiAl Bronze, *Metall. Mater. Trans. A*, 2006, **37A**, p 2239–2251
7. T.R. McNelley, K. Oh-Ishi, and A.P. Zhilyaev, Microstructure Evolution and Microstructure-Property Relationships in Friction Stir Processing of NiAl Bronze, *Mater. Sci. Forum*, 2007, **539–543**, p 3745–3750
8. M.W. Mahoney, W.H. Bingel, S.R. Sharma, and R.S. Mishra, Microstructural Modification and Resultant Properties of Friction Stir Processed Cast NiAl Bronze, *Mater. Sci. Forum*, 2003, **426-432**, p 2843–2848
9. M.D. Fuller, S. Swaminathan, A.P. Zhilyaev, and T.R. McNelley, Microstructural Transformations and Mechanical Properties of Cast NiAl Bronze: Effects of Fusion Welding and Friction Stir Processing, *Mater. Sci. Eng. A*, 2007, **A463**, p 128–137
10. D.R. Ni, P. Xue, D. Wang, B.L. Xiao, and Z.Y. Ma, Inhomogeneous Microstructure and Mechanical Properties of Friction Stir Processed NiAl Bronze, *Mater. Sci. Eng. A*, 2009, **A524**, p 119–128
11. G. Çam, S. Mistikoglu, and M. Pakdil, Microstructural and Mechanical Characterization of Friction Stir Butt Joint Welded 63% Cu-37% Zn Brass Plate, *Weld. J.*, 2009, **88**(11), p 225s–232s
12. G. Çam, H.T. Serindag, A. Çakan, S. Mistikoglu, and H. Yavuz, The Effect of Weld Parameters on Friction Stir Welding of Brass Plates, *Mat.-wiss. u. Werkstofftech.*, 2008, **39**(6), p 394–399
13. R.S. Mishra and Z.Y. Ma, Friction Stir Welding and Processing, *Mater. Sci. Eng. R*, 2005, **R50**(1–2), p 1–78
14. R. Nandan, T. DebRoy, and H.K.D.H. Bhadeshia, Recent Advances in Friction-Stir Welding—Process, Weldment Structure and Properties, *Prog. Mater. Sci.*, 2008, **53**(6), p 980–1023
15. P.L. Threadgill, A.J. Leonard, H.R. Shercliff, and P.J. Withers, Friction Stir Welding of Aluminium Alloys, *Int. Mater. Rev.*, 2009, **54**(2), p 49–93
16. G. Çam and S. Mıstıkoğlu, Recent Developments in Friction Stir Welding of Al-Alloys, *JMEPEG*, 2014, **23**(6), p 1936–1953
17. C.B. Fuller, Friction Stir Tooling: Tool Materials and Design, Friction Stir Welding And Processing, ed. by R.S. Mishra, M.W. Mahoney (ASM International, 2007), p. 7–35
18. G.M. Xie, Z.Y. Ma, and L. Geng, Development of a Fine-Grained Microstructure and the Properties of a Nugget Zone in Friction Stir Welded Pure Copper, *Scripta Mater.*, 2007, **57**(2), p 73–76
19. H.J. Liu, J.J. Shen, Y.X. Huang, L.Y. Kuang, C. Liu, and C. Li, Effect of Tool Rotation Rate on Microstructure and Mechanical Properties of Friction Stir Welded Copper, *Sci. Technol. Weld. Join.*, 2009, **14**(6), p 577–583
20. H.S. Park, T. Kimura, T. Murakami, Y. Nagano, K. Nakata, and M. Ushio, Microstructures and Mechanical Properties of Friction Stir Welds of 60% Cu-40% Zn Copper Alloy, *Mater. Sci. Eng. A*, 2004, **A371**(1–2), p 160–169
21. W.B. Lee and S.B. Jung, The Joint Properties of Copper by Friction Stir Welding, *Mater. Lett.*, 2004, **58**(6), p 1041–1046
22. C. Meran, The Joint Properties of Brass Plates by Friction Stir Welding, *Mater. Des.*, 2006, **27**(9), p 719–726
23. G. İpekoğlu and G. Çam, Effects of Initial Temper Condition and Postweld Heat Treatment on the Properties of Dissimilar Friction-Stir-Welded Joints between AA7075 and AA6061 Aluminum Alloys, *Metall. Mater. Trans. A*, 2014, **45A**(7), p 3074–3087
24. G. İpekoğlu, S. Erim, and G. Çam, Investigation into the Influence of Post-Weld Heat Treatment on the Friction Stir Welded AA6061 Al-Alloy Plates with Different Temper Conditions, *Metall. Mater. Trans. A*, 2014, **45A**(2), p 864–877
25. G. İpekoğlu, S. Erim, and G. Çam, Effects of Temper Condition and Post Weld Heat Treatment on the Microstructure and Mechanical Properties of Friction Stir Butt-Welded AA7075 Al Alloy Plates, *Int. J. Adv. Manuf. Technol.*, 2014, **70**(1–4), p 201–213
26. G. İpekoğlu, S. Erim, and B. Gören, Kıral, and G. Çam, Investigation into the Effect of Temper Condition on Friction Stir Weldability of AA6061 Al-Alloy Plates, *Kovove Mater.*, 2013, **51**(3), p 155–163
27. G. İpekoğlu, B. Gören Kıral, S. Erim, and G. Çam, Investigation of the Effect of Temper Condition on the Friction Stir Weldability of AA7075 Al-Alloy Plates, *Mater. Tehnol.*, 2012, **46**(6), p 627–632
28. G. Çam, G. İpekoğlu, and H. Tarık Serindağ, Effects of Use of Higher Strength Interlayer and External Cooling on Properties of Friction Stir Welded AA6061-T6 Joints, *Sci. Technol. Weld. Join.*, 2014, **19**(8), p 715–720